UNIVERSITY OF MICHIGAN

Michigan Engineering

NERS/BIOE 481

Lecture 09
Nuclear Medicine Detectors

Michael Flynn, Adjunct Prof
Nuclear Engr & Rad. Science
mikef@umich.edu
mikef@rad.hfh.edu

Henry Ford Health System
RADIOLOGY RESEARCH

- General Models

Radiographic Imaging: Subject contrast (A) recorded by the detector (B) is transformed (C) to display values presented (D) for the human visual system (E) and interpretation.

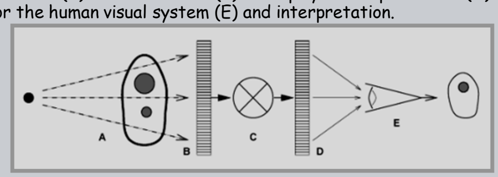

Radioisotope Imaging: The detector records the radioactivity distribution by using a multi-hole collimator.

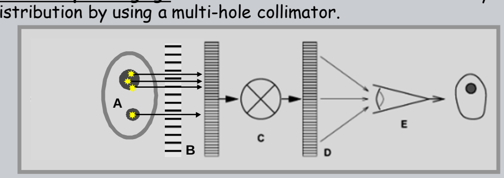

V.B.1 - The Anger Camera (10 charts)

B. Nuclear Medicine Detectors
   1. Physical Design of the Anger camera
      a. Basic components and circuits.
      b. The scintillator crystal.
      c. Optical PMT coupling
      d. PM tubes
      e. Detector gantry.

V.B.1.a - Basic principles and components

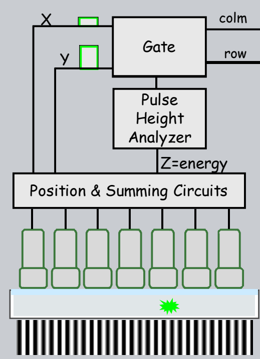

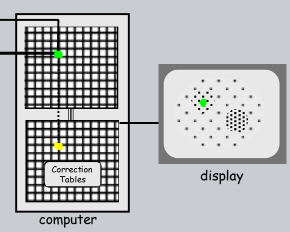

- The Anger camera computes an x,y position for each detected x-ray and increments the count in a corresponding image pixel
- Only events with a full energy sum (Z) in the photo-peak are processed.

V.B.1.b - The scintillation crystal.

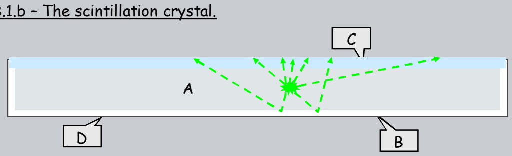

A. A NaI scintillation crystal with thallium doping is typically ¼ to ½ inches thick.
B. The peripheral boundaries are coated with a granular white material to promote reflection of light.
C. The front surface has an optical quality glass sheet from which emitted light is detected.
D. The entire assembly is sealed to prevent moisture from degrading the crystal material

---

V.B.1.c - Optical Photomultiplier tube (PMT) coupling.

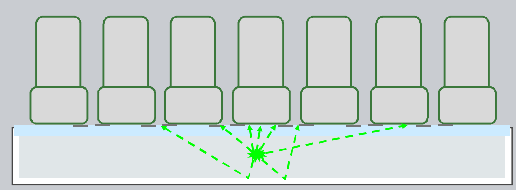

A. Photomultiplier tubes are coupled to the glass window using a coupling grease that has an index of refraction designed to maximize the transfer of light from the crystal thru the glass to the PMT
B. In early designs, filters were place on the glass surface to shape the response of the PMTs.

V.B.1.c – Individual PMT response vs scintilation position.

The response of an individual PMT varies with the relative position of the scintillation event

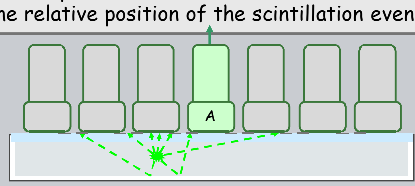

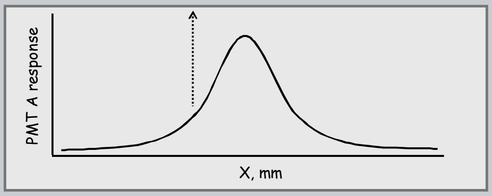

V.B.1.c – PMT placement

- PMTs are placed in an hexagonal array on circular or rectangular crystal assemblies

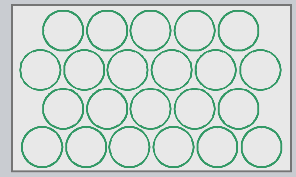

- Hexagonal PMTs placed on a circular crystal with optical coupling grease.

V.B.1.d – PMT basic principle

- A photomultiplier tube is a vacuum tube consisting of an input window, a photocathor and an electron multiplier sealed into an evacuated glass tube.

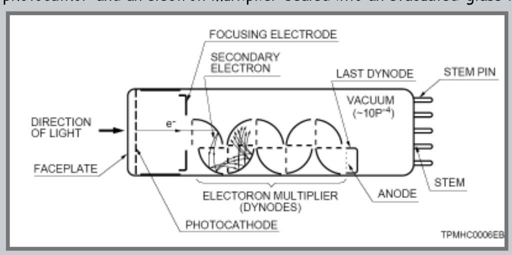

Hammamatsu PMT Handbook

- Light passes through the input window and excites the electrons in the photocathode so that photoelectrons are emitted into the vacuum. Photoelectrons are accelerated and focused by the focusing electrode onto the first dynode where they are multiplied by means of secondary electron emission. This secondary emission is repeated at each of the successive dynodes.The multiplied secondary electrons emitted from the last dynode are finally collected by the anode.

V.B.1.e – Gamma camera detector assembly

- The crystal and PMT assembly is surrounded by 'mu' metal to minimize the influence of magnetic fields.
- The assembly is then mounted in a lead shielded cabinet.

(photos from MUSC)

Detail view showing lead shielding

V.B.1.e – Gamma camera detector assembly

- The detector assembly is often mounted in a gantry providing circular rotation for SPECT examinations.
- Reduced examination time is achieved by using two detectors.

Siemens Symbia E Dual

V.B.1.e – Gamma camera detector assembly

GE Discovery 670 SPECT/CT

Dual Head SPECT imaging systems integrated with an x-ray CT system

Philips SPECT/CT

V.B.1.e – Gamma camera detector assembly

Breast - GE Discovery NM750b

NM systems designed for imaging specific body parts

Heart - GE Discovery NM530c

V.B.2 – Position estimation (21 charts)

B. Nuclear Medicine Detectors
   2. Position estimation for Anger cameras
      a. Response from one PMT
      b. Weighted sum estimation
      c. Uniformity correction
      d. Resolution (error in position estimate)
      e. Maximum Likelihood Estimation (MLE)
      f. Modern commercial design

V.B.2 – Position estimation

The precise estimation of the position of a detected event by using the relative responses of a small set of detectors with poor resolution is fundamental to the operation of nuclear medicine and PET imaging devices.

V.B.2.a – Response from one PMT

The number of electrons recorded by a PMT as a function of the position of incident gamma rays, x, is peaked at the center of the PMT and extends beyond it's edges.

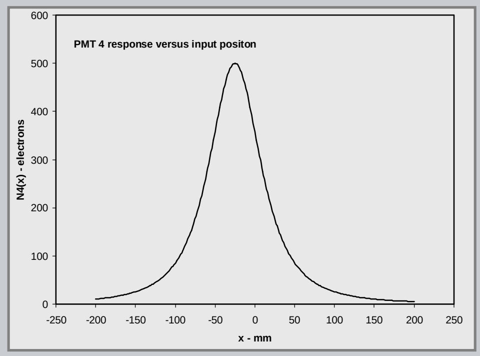

Response of a single 50 mm PMT based on it's solid angle relative to a detector plane 50 mm away (Barrett eq. 5.188)

V.B.2.a – Responses from a set of PMTs

The x and y position estimates are usually determined from 1D analysis based on the positions of the rows and columns of PMTs

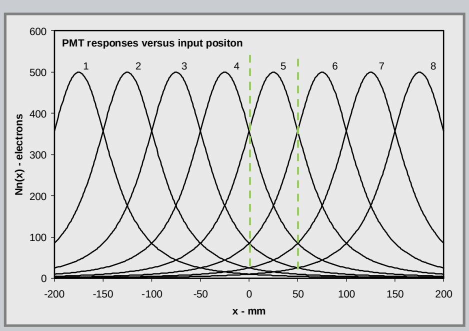

The response of 8 columns of PMTs with 50 mm spacing is illustrated using the shape from the prior slide.

V.B.2.b – Centroid position estimate

A position estimate based on the linearly weighted sum of the eight PMT responses deviates slightly from a linear relation.

An improved estimate is obtained by increasing the weights of the outside tubes by 1.34

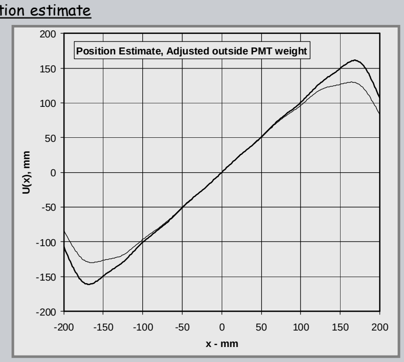

Note: $N_n(x)$ from the prior slides has been normalized by 0.56/500

$$U(x) = \sum_{n=1,8} w_n N_n(x)$$

$$w_n = -175, -125, -75 ... +125, +175$$

V.B.2.b – Centroid position estimate

The sum of the signal from all PMTs is used to estimate the total energy deposition and identify the photopeak for gamma rays of a specific energy..

An improved estimate with 9% variation is obtained by increasing the weights of the outside tubes by 1.34

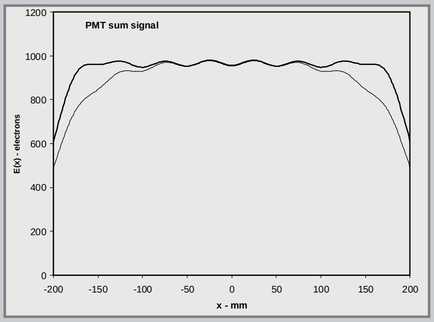

Note: $E(x)$ is computed here in terms of the number of electrons collected. The total of about 960 electron would have a standard deviation of 3.2% and FWHM of 2.35*3.2 = 6.5% which is someone less that usual.

$$E(x) = \sum_{n=1,8} N_n(x)$$

V.B.2.b Original Anger Camera

- The original Anger camera designs used passive electronic circuits to compute position from weighted PMT signals.
- A 7 PMT design is shown (Anger 1958) in which the charge from each PMT is collected on a capacitor. The capacitance value is proportional to the PMT weight.

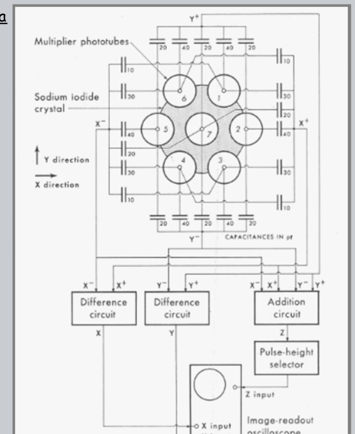

From Hine, Vol 1, 1967

V.B.2.b – Transformed PMT response

- A common prior design used 37 PMTs of 2" or 3" diameter arranged over a circular NaI crystal.
- This photo illustrates a masking plate used to position each PMT.

- The shape of the PMT response curve can be altered by a mask pattern placed between the PMT and the NaI crystal. This can improve the linearity of position estimates.
- A disadvantage is that the number of collected electrons is reduced and the precision of the position estimate is worse.
- Non-linear weighting circuits using delay-line elements were introduced to shape the response without loss of resolution.

V.B.2.b – Digital camera logic

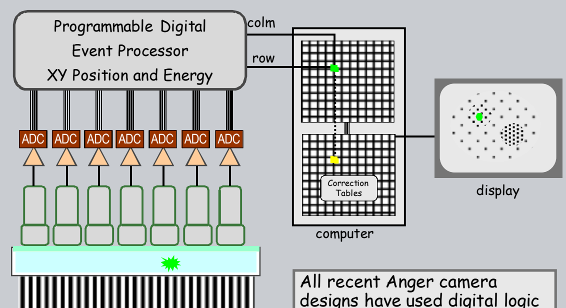

Figure adapted from slide #3

All recent Anger camera designs have used digital logic circuits to compute the X and Y position of each event and the Energy in relation to a defined energy window.

V.B.2.c – Uniformity correction

United States Patent	4,212,061
Knoll et. al.	July 8, 1980

RADIATION SIGNAL PROCESSING SYSTEM

Inventors: Glenn F. Knoll, Ann Arbor;
Donald R. Strange, Howell;
Matthew C. Bennett, Jr, Ann Arbor, MI.

"Coordinate signals X, Y are corrected to their true coordinate U, V values respectively by accessing translation table rectangular matrix arrays containing U,V values addressed by their respective corresponding X,Y coordinates, .."

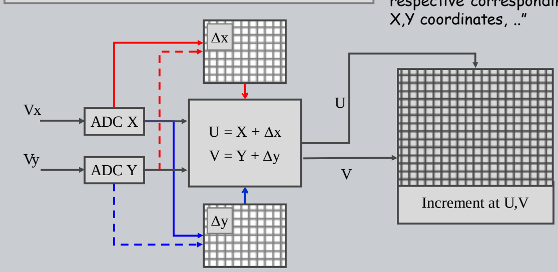

V.B.2.d – Resolution

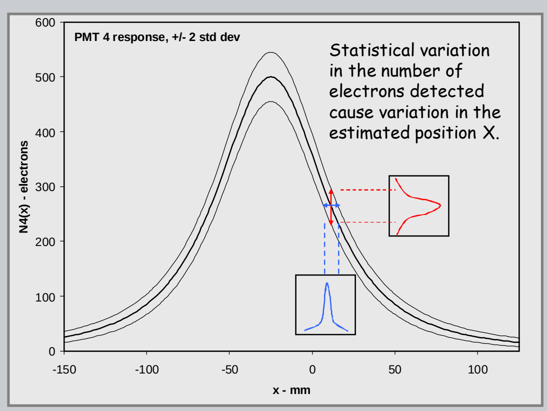

V.B.2.d – Resolution

- Variation in the estimate position (x, y) of a detected gamma ray results from statistical noise in the number of electrons collected from each PMT.
- For the centroid estimate shown in slide 18, the estimated X position comes from the observed set of PMT electron signals (N_i, $i=1,8$) . In the estimate below this is X rather than U(x) .
- The variance of this is computed using propagation of error.
- The spatial resolution in FWHM is then equal to $2.35\sigma_x$

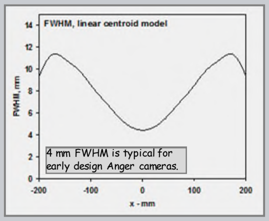

$$X = \sum_{i=1,8} w_i N_i$$

$$(\sigma_x)^2 = \sum_{i=1,8} w_i^2 N_i$$

The FWHM based on the weights used earlier is shown at the left. Poor resolution at the sides results from the high weight values for the outside tubes. This can be avoided by using local estimates with weights adjusted for the approximate position

V.B.2.d – PMT Position Probability distribution

If the mean number of electrons observed from PMT i for a gamma ray detected at position x is $N_i(x)$,

then the conditional probability of observing n_i electrons, $P[n_i|x]$, is expected to follow a Poisson distribution as was discussed in lecture 05 (or the approximate Gaussian).

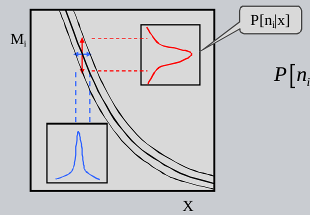

$$P[n_i \mid x] = \frac{(N_i(x))^{n_i} e^{-N_i(x)}}{n_i!}$$

$$\cong \frac{1}{\sigma_n \sqrt{2\pi}} e^{-\left((N_i(x)-n_i)\big/ 2\sigma_n^2\right)}$$

V.B.2.e – Maximum Likelihood

- If we consider the conditional probabilities associated with each PMT, then the likelihood expression is defined as the product of each.

$$P[n_1, n_2, \ldots n_j, \mid x] = \prod_{i=1}^{j} P[n_i \mid x]$$

- The maximum likelihood in relation to x can then be taken as as an optimal estimate of the photon interaction position.
- It has been shown that maximizing the log likelihood is equivalent to maximizing the likelihood. This is done by finding the value of x for which the derivative is zero. Using the Poisson distribution, this can be written as.

$$\frac{\delta}{\delta x} \ln\left(P\left[n_1, n_2, \ldots n_j, \mid x\right]\right) = \sum_{i=1}^{j} n_i \frac{\delta\left(N_i(x)\right)/\delta x}{N_i(x)} - \frac{\delta}{\delta x} \sum_{i-1}^{j} N_i(x) = 0$$

V.B.2.e – Maximum Likelihood

- Clinthorne (IEEE, TNS 1987) shows that the prior equation can be rearranged as a sum of terms linear in n_i ,

$$0 = \sum_{i=1}^{N} n_i \left[\frac{\delta\left(N_i(x)\right)/\delta x}{N_i(x)} - e(x)\right] = \sum_{i=1}^{N} n_i p_i(x) \quad , \quad e(x) = \frac{\sum_{j=1}^{j} \delta\left(N_j(x)\right)/\delta x}{\sum_{k=1}^{j} N_k(x)}$$

- The second term of the weighting factor, $e(x)$, compensates for changes in total light collection and is small except at the edges.
- The weighting factor, $p_i(x)$, is a function of x approximately equal to the derivative of the PMT response function (see Barrett Fig 5.49).
- The value of x for which this weight sum is zero is the maximum likelihood estimate of the position of the detected gamma ray.
- The variance, which dictates the resolution is otherwise shown to be equivalent to equation 5.205 in Barrett.

$$(\sigma(x))^2 = \left[\sum_{i=1}^{j} \frac{\left(\delta\left(N_i(x)\right)/\delta x\right)^2}{N_i(x)}\right]^{-1}$$

V.B.2.e – Maximum Likelihood

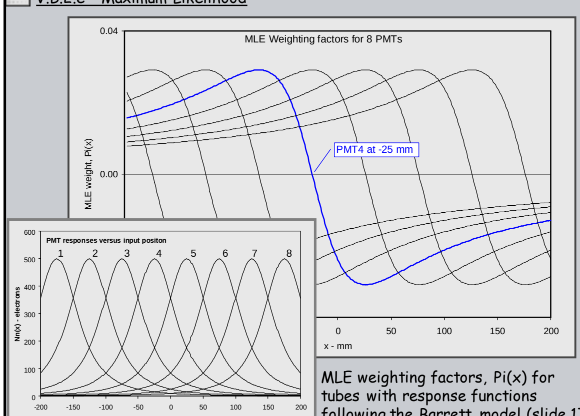

MLE weighting factors, Pi(x) for tubes with response functions following the Barrett model (slide 17).

V.B.2.e – Maximum Likelihood

$N_i(x)$ for 8 PMTs (from slide 18)

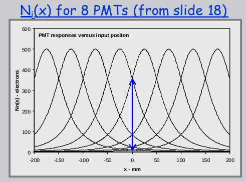

$p_i(x)$ for 8 PMTs (from slide 30)

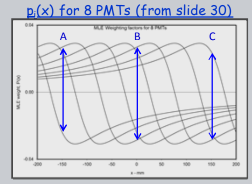

- If the observed n_i values are equal to the mean number of electrons N_i for each tube, the MLE sum as a function of x is seen to be zero for x=0. (i.e. no statistical fluctuations)
- For actual values of n_i observed for a detected gamma ray, we would find the value of x for which the MLE sum is zero.

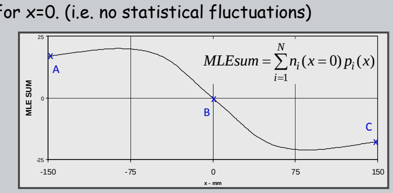

V.B.2.e – Maximum Likelihood

- As an illustration, consider a system with 7 PMTs at 50 mm intervals. Each have Gaussian response functions with a FWHM of 50 mm:

$$N_i(x) = N_{\max} e^{-\left(\frac{x-50i}{W}\right)^2} \qquad W = \frac{50}{2\sqrt{.693}}$$

- From pg. 28, ignoring the $e(x)$ term we seek a solution to:

$$0 = \sum_{i=-3}^{i=3} \left(\frac{\delta N_i(x)}{\delta x} \Big/ N_i(x) \right) n_i$$

- For the Gaussian shape function, the derivative is:

$$\frac{\delta N_i(x)}{\delta x} = -N_i(x) 2 \left(\frac{x-50i}{W^2} \right)$$

- And the MLE equation becomes

$$0 = \sum_{i=-3}^{3} \left\{ -2n_i \left(\frac{x-50i}{W^2} \right) \right\}$$

V.B.2.e – Maximum Likelihood

- The MLE equation is then solved by separating the two terms in the summation and rearranging:

$$0 = -\sum_{i=-3}^{3} \left\{ 2n_i \frac{x}{W^2} \right\} + \sum_{i=-3}^{3} \left\{ 2n_i \frac{50i}{W^2} \right\}$$

$$\frac{2}{W^2} x \sum_{i=-3}^{3} n_i = \frac{2}{W^2} 50 \sum_{i=-3}^{3} n_i i$$

$$x = 50 \frac{\sum_{i=-3}^{3} n_i i}{\sum_{i=-3}^{3} n_i}$$

- Interestingly, for Gaussian response functions, the MLE solution reduces to a simple centroid the same as the traditional Anger method.
- For a set of n_i values equal to [2, 3, 15, 183, 272, 20, 5] we get:

$$x = 50 \frac{300}{500} = 30\ mm$$

V.B.2.e – Maximum Likelihood

- For actual PMT response functions the MLE method is significantly better.
- The experimental performance reported by Clinthorne (IEEE, TNS 1987) indicates the the resolution in FWHM is about 30% larger for a traditional centroid estimate in relation to a Maximum Likelihood estimate.
- Position estimates from Maximum Likelihood estimates are otherwise seen to be linear with true position.

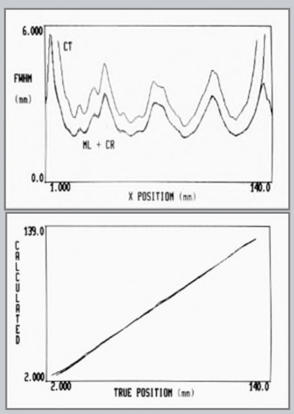

V.B.2.f – Modern commercial design

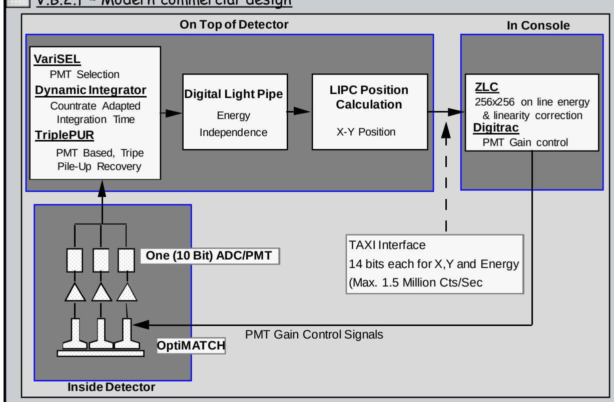

The Siemens H3 design illustrates the digital detector functions provided by most commercial systems.

V.B.2.f – linearity and resolution

From W.D. Erwin

- Modern gamma cameras with proper calibration provide good resolution and linearity.
- Bar pattern phantoms are used routinely to verify proper calibration.

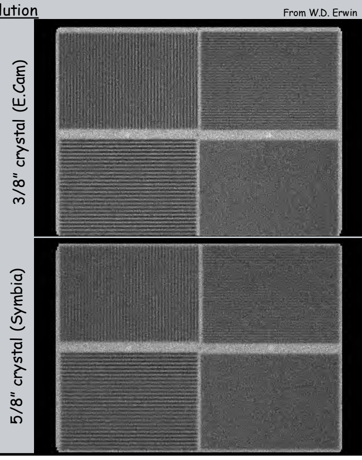

V.B.3 – Other devices (19 charts)

B. Nuclear Medicine Detectors
  3. Other gamma camera devices
    a. Segmented crystal designs.
    b. Drift photodiodes.
    c. CdZnTe (CZT) cameras.

V.B.3.a – segmented crystal designs

- Early gamma camera designs using segmented scintillation crystals were handicapped by the need to use PM tubes to detect light.
- In 1960 Bender and Blau explored an alternative type of scintillation camera called an "auto-fluoroscope." Their detector was a mosaic of collimated sodium iodide crystals instead of a large single crystal. Unlike the Anger camera, which is now in common use, the auto-fluoroscope (Baird Atomic multicrystal camera) had limited application.

The Baird multi-crystal camera used 293 crystals, 3/8 inch in diameter, arranged in a flat mosaic pattern. Gamma ray event positions were determined using light pipes to each crystal and photomultiplier tubes.

V.B.3.a – Breast Specific Gamma Imaging (BSGI)

Dilon 6800

- 3 mm square segmented detector crystals (3000+)
- 48 position sensitive PMTs
- High resolution in a small field of view.

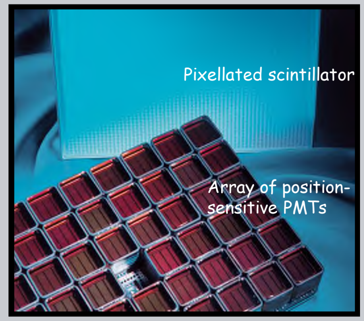

www.dilon.com

V.B.3.a – Breast Specific Gamma Imaging (BSGI)

Dilon 6800

- The crystals and PMTs are packaged in a maneuverable detector measuring 6" x 8" x 4" which can be placed in direct contact with the breast and chest wall.
- The resolution has the potential to provide early detection of small lesions.

www.dilon.com

V.B.3.a – Breast Specific Gamma Imaging (BSGI)

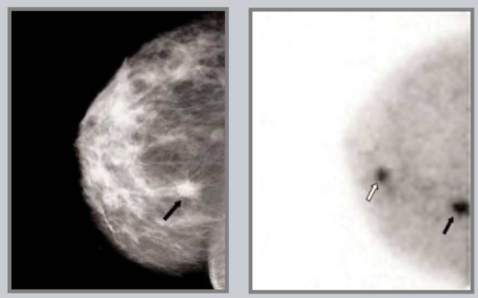

A second tumor, not detected in the mammogram, is identified in a breast radioisotope image.

V.B.3.b – CsI & photodiode array

- Cameras using PMTs have generally been designed with NaI.
- NaI scintillators have a spectral emission that is well matched to the response of PMT detectors (QE about .3 to .35 %).

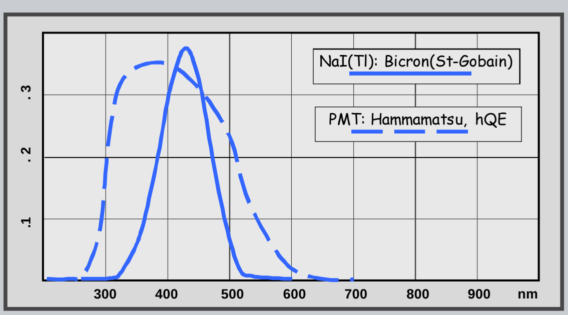

V.B.3.b – CsI & photodiode array

- Cameras using silicon photodiode detectors rather that PMTs have been more recently considered (Engdahl/Knoll USP#5171998).
- CsI scintillators have a spectral emission that is well matched to the response of silicon diodes

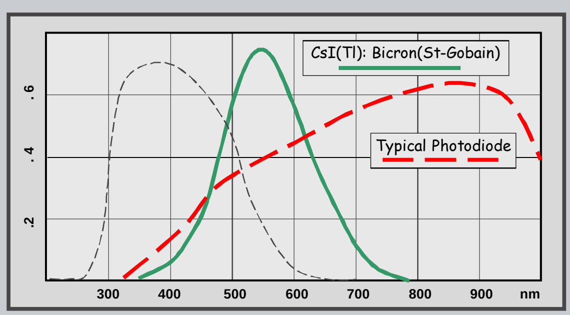

V.B.3.b – CsI & photodiode array

Each of the 4,096 CsI(Tl) scintillation crystals is viewed by a single small photodiode

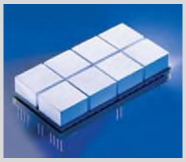

Normal Hand Technetium 99m

The DigiRad 2020tc Imager™ detector size is 21 cm x 21 cm (8 x 8 inches), and the leading edge dead space is 1.3 cm (0.5 inches). This detector size is smaller than most commercially-available gamma cameras today.

V.B.3.b – CsI & photodiode array

Siman W, Kappadath SC; Performance characteristics of a new portable gamma camera, Med. Phys. 39 (6), June 2012.

Digirad Ergo Camera

- CsI pixelated crystal (3mm x 3mm x 6mm)
- Resolution measured with Tc99m filled capillary tubes
- Offset tubes used to obtain LSF with sub-pixel spacing

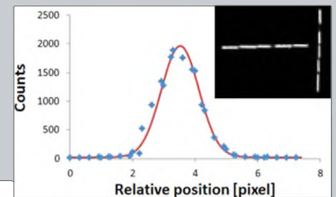

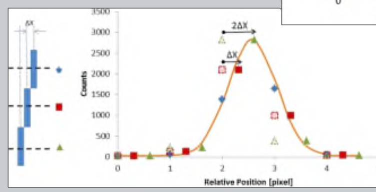

V.B.3.b – CsI & photodiode array

Siman W, Kappadath SC; Performance characteristics of a new portable gamma camera, Med. Phys. 39 (6), June 2012.

Digirad Ergo Camera

- CsI pixelated crystal (3mm x 3mm x 6mm)
- Resolution measured with Tc99m filled capillary tubes

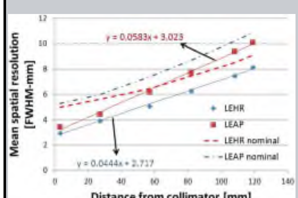

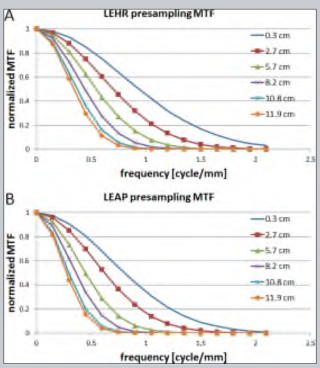

V.B.3.b – CsI & photodiode array

- Conventional photodiodes with large area have large input capacitance that leads to excessive noise.
- Silicon Drift Diodes (SDD) avoid this by 'drifting' the collected electrons to a small area anode. The small anode area greatly reduces the device capacitance providing for low noise detector circuits.

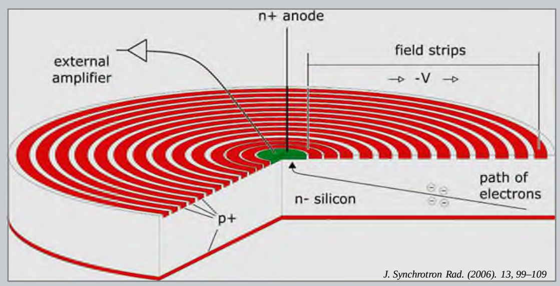

J. Synchrotron Rad. (2006). 13, 99–109

V.B.3.b – CsI & photodiode array

SDDs can be fabricated into an hexagonal array structure and used with CsI as an Anger camera. Fiorini reported this experimental 19 SDD device.

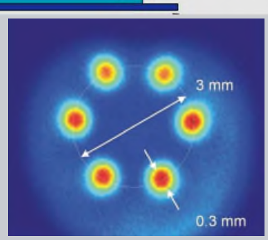

J. Synchrotron Rad. (2006). 13, 99–109

V.B.3.b – CsI & photodiode array

The HICAM Gamma Camera

"The use of .. SDDs as scintillator photodetectors, characterized by high quantum efficiency and low electronic noise, is the unique aspect of this camera. … [Prototypes] provide a high intrinsic spatial resolution (< 1 mm), system spatial resolution of ~2.67 mm @ 4 cm and appropriate sensitivity."

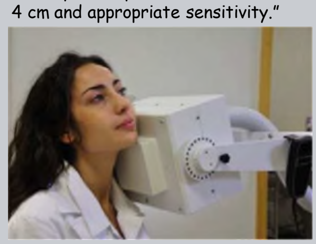

Thyroid Images

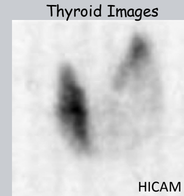

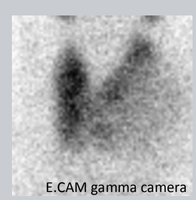

IEEE TNS, VOL. 59, NO. 3, JUNE 2012

V.B.3.c – Solid State CZT arrays

CZT module, Univ. of Arizona

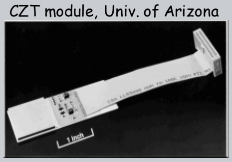

Solid state detectors have recently been considered for gamma camera applications, particularly detectors using Cadmium Zinc Telluride (CZT).

Prototype CZT camera (GE Medical) tested at the Mayo Clinic.

Mueller, J. Of Nucl. Med., 44, 4, 2004

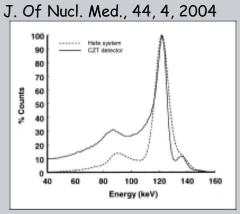

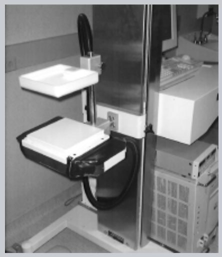

V.B.3.c – Solid State CZT arrays

D-SPECT cardiac system.
Gambhir, JNM, April 2009

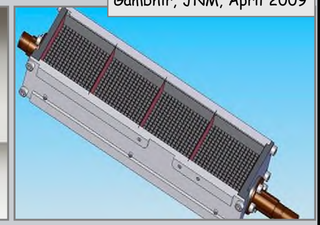

Detector column:

- CZT sensor (39 · 39 · 5 mm)
- four 16 · 16 pixel detectors
- Square hole tungsten collimator
  - pitch, 2.46 mm
  - length, 21.7 mm
  - septa 0.2 mm).

V.B.3.c – Solid State CZT arrays

GE Alcyone technology.
Herzog, JNM, Jan 2010

The modular CZT technology is now used in a commercial product, the GE Discovery NM 530c, that achieves fast cardiac imaging using an optimized geometry.

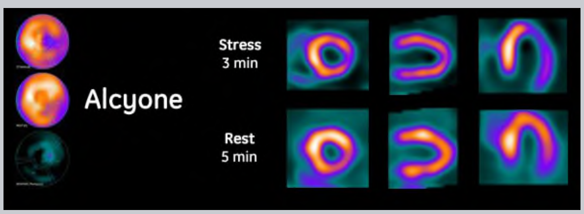

V.B.3.c – Solid State CZT arrays

Molecular Dynamics has a license for use of the D-SPECT CZT detector technology for whole body imaging applications..

Multiples Detector motions rotation, radial, & swivel

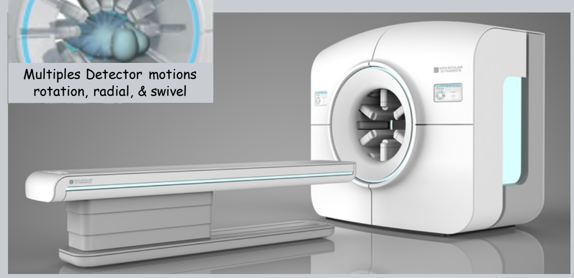

Molecular Dynamics Valiance x12
Goshen et al. EJNMMI Physics (2018)

V.B.3.c – Solid State CZT arrays

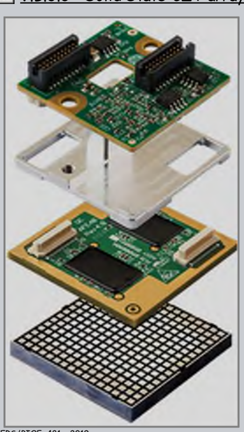

GE Healthcare

Digital CZT Detectors
Center of Excellence

Rehovot, Israel

GE has recently made significant investments to establish manufacturing facilities for CZT crystal growth, signal readout, and detector module integration.

Rehovot, GE Healthcare - YouTube

V.B.3.c – Solid State CZT arrays

GE Discovery 670 CZT

Introduced in 2017

V.B.3.c – Solid State CZT arrays

GE Discovery 670 CZT

V.B.3.c – Solid State CZT arrays

GE Discovery 670 CZT

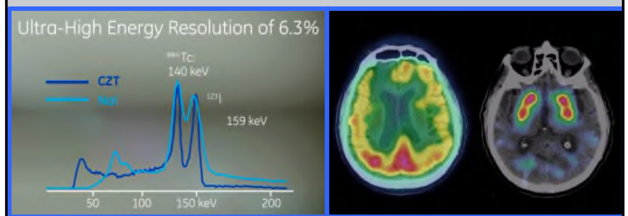

The improved spectral resolution of the CZT detector compared to conventional NaI detector resolved 123I and 99mTc full energy peaks.

DaTscan 123-I and Ceretec 99m-Tc studies completed simultaneously to assess signs of demential and Parkinson's disease.

V.B.4 – PET Systems (32 charts)

B. Nuclear Medicine Detectors
  4. Designs for PET Systems
    a. Pharmaceutical production. (6 charts)
      - Radioisotopes.
      - Medical Cyclotrons.
      - Radiochemistry.
    b. PET Cameras. (11 charts)
      - Detection Geometry, 2D & 3D.
      - Scintillators & resolution.
      - Time of Flight.
    c. Advanced concepts. (18 charts)
      - Radial elongation & interaction depth.
      - Silicon Photo-Multipliers (SiPM).
      - Advanced SiPM PET systems.

V.B.4.a – Radioisotopes

Common Radioisotopes for PET imaging

Isotope	Half life	Production	Chemistry
^{18}F	2 hours	cyclotron	Very Good (replaces H)
^{15}O, ^{11}C, ^{13}N	2 – 20 min	cyclotron	Excellent
^{82}Rb	2 min	generator	OK (like Na & K)

Adapted from; Moses, 1/26/2007 ppt

V.B.4.a – Radioisotopes

Examples of [18F] Tracers

Tracer	Molecular Level	Disease Level	Example
18F FTHA (fatty acid)	Anaerobic metabolism	Cardiology	Ischemia
Fluoromisonidazole	Hypoxia	Oncology	Poorly perfused tumors
Methylbenperidol	Dopaminergic D2 receptor	Psychiatry	Schizophrenia, Addiction
Methylspiperone	Dopaminergic D2 receptor	Psychiatry	Schizophrenia, Addiction
Fluorostradiol	Steroid metabolism	Oncology	Estrogen Dependent Breast Cancer
Altanserine	Seratonergic S2 receptor	Psychiatry	Depression
FLT Fluoro-L-Thymidine	DNA synthesis	Oncology	Tumor proliferation
FDG	Glucose metabolism	Oncology Cardiology Neurology	Lung Cancer, Myocardial Viability, Alzheimer's

Adapted from; GE Healthcare, TRACERlab FXf-n

V.B.4.a – Radioisotopes

Sketch of $H_2{}^{18}O$ target system used at Julich (FRG) for production of ^{18}F via the $^{18}O(p, n)^{18}F$ process.

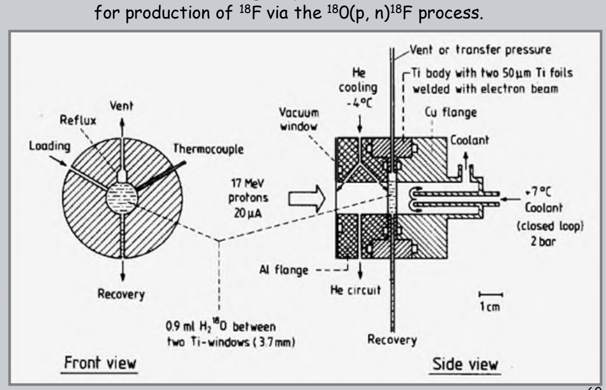

from; Qaim, NIM, 1989

V.B.4.a – Medical Cyclotrons

The cyclotron, one of the earliest types of particle accelerators, makes use of the magnetic force on a moving charge to bend moving charges into a semicircular path between accelerations by an applied electric field. The applied electric field accelerates electrons between the "dees" of the magnetic field region. The field is reversed at the cyclotron frequency to accelerate the electrons back across the gap.

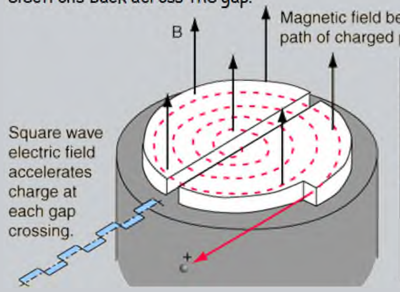

While the radius increases with energy, the time to complete one orbit is constant. The acceleration frequency is therefore constant

$$\omega_{cyclotron} = \frac{qB}{m}$$

from: hyperphysics

V.B.4.a – Medical Cyclotrons

The PET medical cyclotron at Stanford University

Interior view of the GE PETtrace medical cyclotron

V.B.4.a – Radiochemistry

Radiopharmaceutical production is done within a 'hot cell' using remote manipulators.

Automated FDG production system (GE Tracerlab) shown within a hot cell (UC Davis).

hot cells, Zurich, Inst. Radioph. Sc.

V.B.4 – PET Systems (32 charts)

B. Nuclear Medicine Detectors
4. Designs for PET Systems
   a. Pharmaceutical production. (6 charts)
      - Radioisotopes.
      - Medical Cyclotrons.
      - Radiochemistry.
   b. PET Cameras. (11 charts)
      - Detection Geometry, 2D & 3D.
      - Scintillators & resolution.
      - Time of Flight.
   c. Advanced concepts. (18 charts)
      - Radial elongation & interaction depth.
      - Silicon Photo-Multipliers (SiPM).
      - Advanced SiPM PET systems.

V.B.4.b – PET Detectors

Ring of Photon Detectors

- Radionuclide decays, emitting e^{+}.
- e^{+} annihilates with e^{-} from tissue, forming back-to-back 511 keV photon pair.
- 511 keV photon pairs detected via time coincidence.
- Positron lies on line defined by detector pair (known as a *chord* or a *line of response* or a *LOR*).

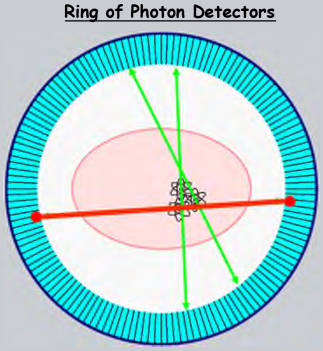

- Detect Pairs of Back-to-Back 511 keV Photons
- No Collimator Needed -> High Efficiency

Adapted from; Moses, 1/26/2007 ppt

V.B.4.b – PET Detectors

Early PET Detectors

- Single crystal coupled to small PMT.
- Single ring and segmented multiple ring designs.

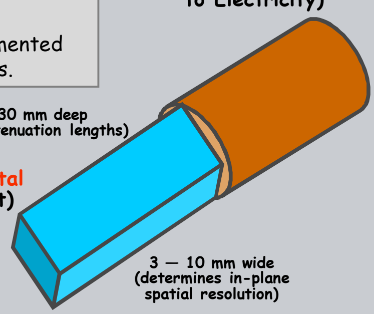

Adapted from; Moses, 1/26/2007 ppt

Multi-Layer PET Cameras

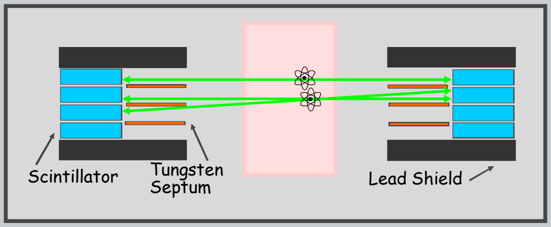

- Can image several slices simultaneously
- Can image cross-plane slices
- Can remove septa to increase efficiency ("3-D PET")

Planar Images "Stacked" to Form 3-D Image

Modern PET Detectors

Block Detector
- Segmented LSO crystals.
- 4 PMT detectors.
- Position from Anger logic
- Siemens HiRez

Hexagonal Detector
- Segmented LYSO crystals.
- Hex PMT detector arrays.
- Philips Pixelar

PET scintillators – stopping power and timing

	LSO	LYSO	GSO	BGO	LuAP	$LaBr_3$
Attenuation Length	1.15	1.2	1.4	1.04	1.04	2.1
Energy resolution	11%	10%	10%	13%	7-9%	3%
Light Yield	1.0	1.2	< 0.5	< 0.2	0.5	2.0
Decay Time	40 ns	40 ns	60 ns	300 ns	17 ns	35 ns
Timing Resolution	450 ps	450 ps	na	na	500 ps	400 ps

LSO - Lu_2SiO_5:Ce
LYSO - Lu[Yt 10%]$_2SiO_5$:Ce
GSO - Gd_2SiO_5:Ce
LuAP - $LuAlO_3$:Ce

LYSO has previously been used because of availability and cost

The improved light emission of LSO relative to that for BGO, that was used in earlier PET systems, produces better position estimates and resolution

Siemens PET

A. BGO scintillator. B. LSO scintillator (HiRez)

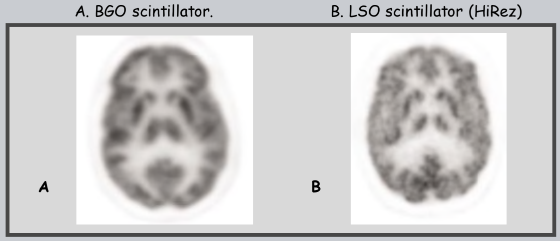

c = 300 mm/ns

Time-of-Flight in PET

- Can localize source along line of flight.
- Time of flight information reduces noise in images.
- Time of flight cameras built in the 80's with BaF2 and CsF.
- These scintillators forced compromises that prevented TOF from flourishing.
- TOF now commercially available using LYSO.

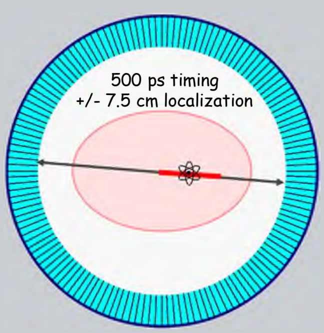

- Variance Reduction Given by $2D/c\Delta t$
- 500 ps Timing Resolution -> 5x Reduction in Variance!

c = 300 mm/ns

The timing coincidence of a PET system with LYSO detector crystals was recently reported as 544 ps FWHM (2011).

Bettinardi et. al., Physical Performance of the new hybrid PET/CT Discovery-690, Med. Phys. 38 (10), Oct. 2011.

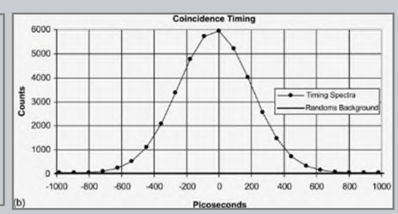

- The D-690 is a multi-ring system with 13,824 LYSO crystals with dimensions of 4.2x6.3x25 mm^3.
- The detection unit is a block of 54 (9x6) individual LYSO crystals coupled to a single square photomultiplier tube with 4 anodes.
- The D-690 has 24 rings of detectors for an axial field of view (FOV) of 157 mm. The transaxial FOV is 70 cm.

GE PET/CT Discovery 690

Time of Flight – effect of timing resolution

More precise localization of annihilation event improves the noise in the reconstructed image

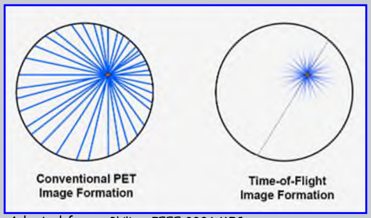

Adapted from : Philips, IEEE 2006 MIC

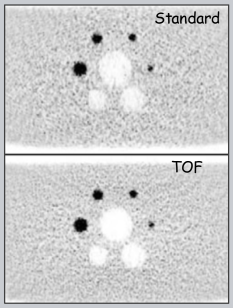

Bettinardi 2011, Discovery 690

Example from University of Pennsylvania

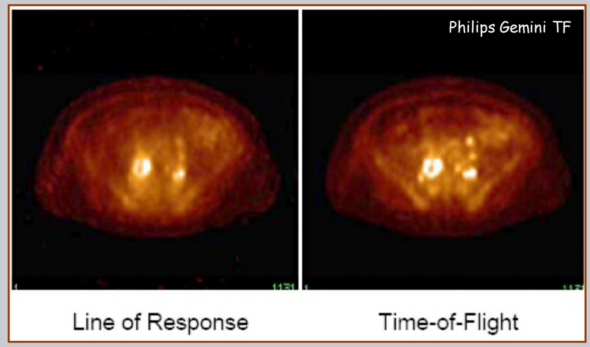

Adapted from : Philips, IEEE 2006 MIC

14 mCi FDG, Philips Gemini TF

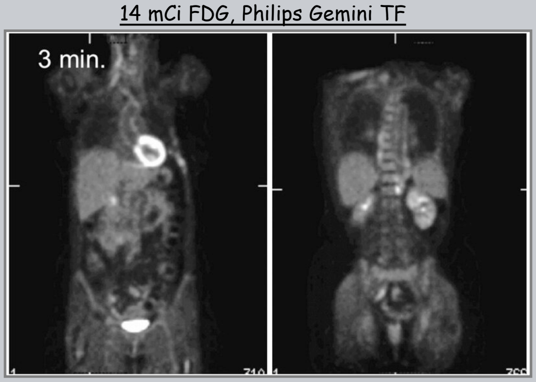

From: Surti, JNM, 3/2007

Commercial time-of-flight PET systems

	Ingenuity TF [40]	Biograph mCT [13]	Discovery 690 [14]	Vereos Digital [41]	Celesteion [43]
Scintillator	LYSO	LSO	LYSO	LYSO	LYSO
Photo-detector	PMT	PMT	PMT	dSiPM	PMT
Crystal size, mm^3	4×4×22	4×4×20	4.2×6.3×25	4×4×19	4×4×12
Total crystals	28,336	32,448	13,824	23,040	30,720
Patient bore, cm	71.7	78	70	70	88
Axial length, cm	18	21.8	15.7	16.4	19.6
Resolution, mm					
Transaxial					
at 1 cm/10 cm	4.8/5.1	4.4/4.95	4.7/5.06	4.1/4.5	5.1/5.1
Axial					
at 1 cm/10 cm	4.73/5.23	4.4/5.9	4.74/5.55	3.96/4.3	5.0/5.4
Energy resolution, %	11.1	11.5	12.4	11.1	NA

Recent developments in time-of-flight PET
Vandenberghe *et al. EJNMMI Physics* (2016)

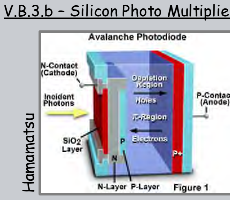

Fiorini, SPIE 4141, 2000

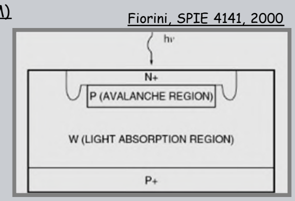

Avalanche Photo Diode (APD)

The depletion layer (P-N) in an APD is relatively thin, resulting in a very steep localized electrical field across the narrow junction.

- At high bias voltage, electrons generated in the p layer continue to increase in energy as they undergo multiple collisions in the silicon lattice.
- This "avalanche" of electrons eventually results in electron multiplication analogous to the process occurring in the dynodes of a photomultiplier tube.

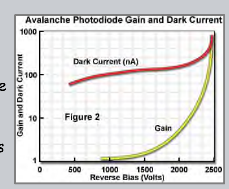

http://hamamatsu.magnet.fsu.edu/articles/avalanche.html

V.B.4.c – Analog SiPM (aSiPM)

Philips Digital Photon Counting, 2012

Single APD
- fully analog
- poor timing
- high bias voltage (up to 1500 V)
- moderate gain (<100)

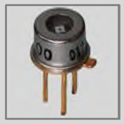

If the APD is operated at a voltage above the breakdown voltage, the avalanche is saturated and the device operates in the 'Geiger' mode.

Geiger-mode APD Arrays (SPAD, SiPM):

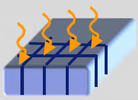

- single photon resolution
- binary, but *still analog*
- better timing
- higher gain (10^6)

http://sensl.com/products/sipmarrays/

V.B.4.c – Digital SiPM (dSiPM)

Philips Digital Photon Counting, 2012

Analog SiPM

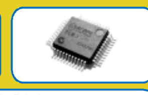

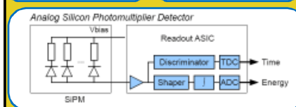

- discrete, limited integration
- analog signals to be digitized
- dedicated ASIC needed
- not scalable

Digital SiPM

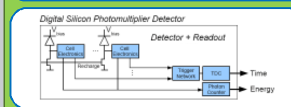

- fully integrated
- fully digital signals
- no ASIC needed
- fully scalable

V.B.4.c – Digital SiPM (dSiPM)

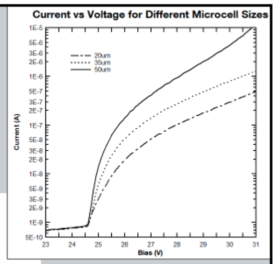

A typical SiPM has microcell densities of between 100 and several 1000 per mm^2. Each microcell operates at high bias with the avalanche saturated at high charge (i.e. 'Geiger' mode).

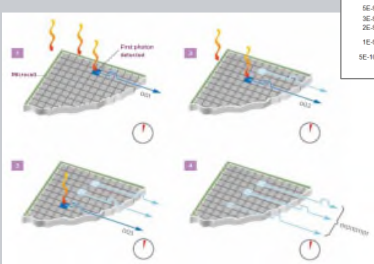

Each incident light photon produces a logical count. For each event, the count of all incident photons is output along with the exact time of the event.

V.B.4.c – dSiPM PET Prototype

Degenhardt, PDPC, 2013

10 Modules, 20 cm FOV

4x4x22 mm3 LYSO crystals

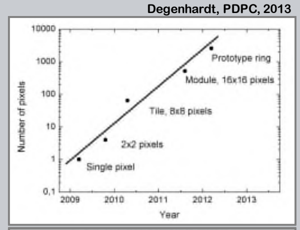

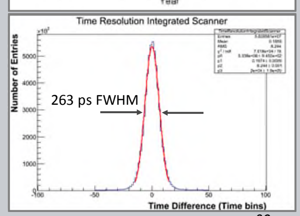

V.B.4.c – SiPM PET Systems

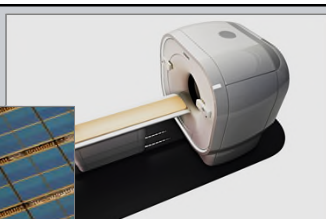

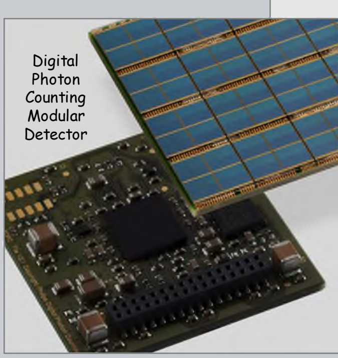

Digital Photon Counting Modular Detector

Philips Vereos PET/CT announced in Dec. 2013

V.B.4.c – SiPM PET Systems

Philips Vereos PET/CT announced in Dec. 2013

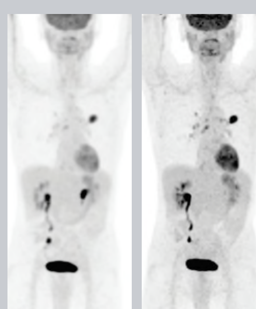

Analog PET | Digital PET

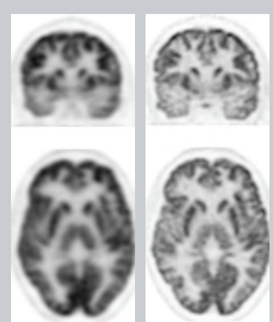

Analog PET | Digital PET

V.B.4.c – SiPM PET Systems

GE Discovery MI
Introduced 2016

V.B.4.c – SiPM PET Systems

GE Discovery MI

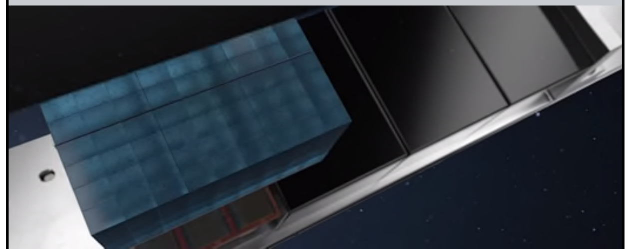

Each detector blocks, has a 4x9 array of Lutetium-Yttrium Oxyorthosilicate (LYSO) crystals coupled to a 3x6 array of silicon photomultipliers (SiPMs) with Anger multiplexing for crystal identification.

- The crystal elements used in the system are 3.95 mm x 5.3 mm x 25 mm.
- Each Hamamatsu SiPM array has 2 x 3 pixels with an active area of 4 mm x 6 mm.

http://www.hamamatsu.com/jp/en/community/optical_sensors/technology/silicon_photomultipliers_sipm/index.html

V.B.4.c – SiPM PET Systems

GE Discovery MI

- The averaged full-width half max (FWHM) of the radial/tangential/axial spatial resolution reconstructed with FBP at 1, 10, and 20 cm from the system center are, respectively,
  - 01cm: 4.10 4.19 4.48 mm,
  - 10cm: 5.47 4.49 6.01 mm, and
  - 20cm: 7.53 4.90 6.10 mm.
- The average photopeak energy resolution is 9.40% FWHM

Hsu et al, J. Nucl. Med. April 2017

V.B.4.c – SiPM PET Systems

GE Discovery MI

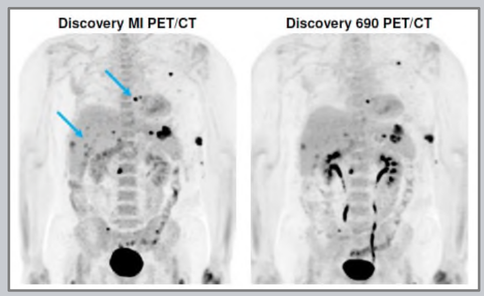

GE LYSO d Si PM (left) GE LYSO PMT (right)

Hsu et al, J. Nucl. Med. April 2017

V.B.4.c – Blur from Radial Elongation

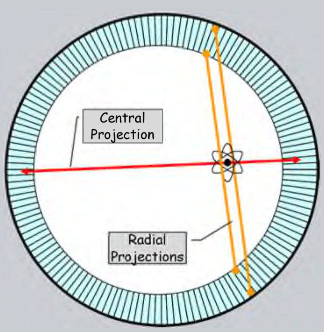

- Penetration of 511 keV photons into crystal ring blurs measured position.
- Blurring worsens as detector's attenuation length increases.
- Also known as *Parallax Error* or *Radial Astigmatism*.
- Can be removed (in theory) by measuring depth of interaction.

From: William W. Moses
Lawrence Berkeley Nat. Lab.
Dept. of Functional Imaging

V.B.4.c – Blur from Radial Elongation

Point Source Images in 60 cm Ring Diameter Camera

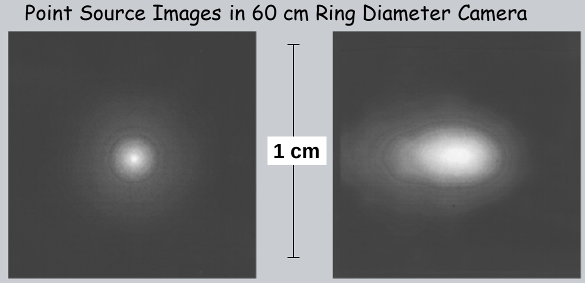

Near Tomograph Center 14 cm from Center

Resolution Degrades Away From Center...

From: William W. Moses
Lawrence Berkeley Nat. Lab.
Dept. of Functional Imaging

V.B.4.c – Improved reconstruction using the PSF

Siemens HD-PET, introduced in 2008, uses the shape of the detected PSF to improve the estimate of the line of response (LOR) and achieve 2mm F18 FWHM

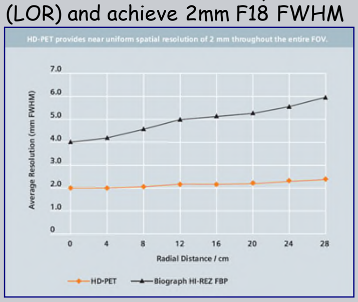

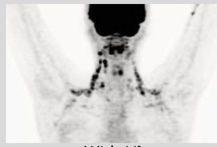

With HD

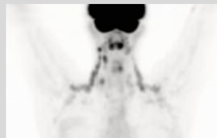

Without HD

V.B.4.c – Depth-encoding PET detector module

Du et. al. Phys. Med. Biol. Feb 2018 (BME Dept., UC Davis)

.. *Depth-encoding PET detector module using SiPM arrays*

The goal of this study was to exploit the excellent spatial resolution characteristics of a position sensitive silicon photomultiplier (SiPM) and develop a high-resolution depth-of-interaction (DOI) encoding positron emission tomography (PET) detector module.

The detector consists of:

- a 30 × 30 array of 0.445mm × 0.445mm × 20mm polished LYSO crystals
- coupled to two 15.5mm × 15.5mm linearly graded SiPM arrays at both ends.

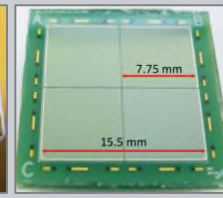

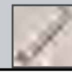

Note: LYSO is a clear crystal. The color in this photograph comes from the background

V.B.4.c – Depth-encoding PET detector module

Du et. al., PMB, Feb 2018

Figure 3. Experimental setup for DOI resolution measurements. Distance and object size are not to scale.

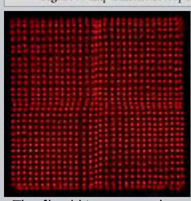

The flood histograms show that all the crystals in the LYSO array can be resolved.

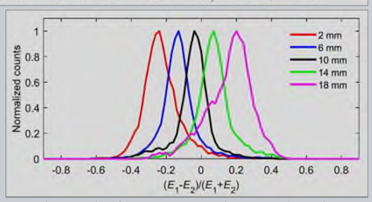

The Depth of Interaction is determined by the difference in energy signal from the top and bottom SiPM to a resolution of 3.8 mm (20 mm length).

V.B.4.c – EXPLORER project

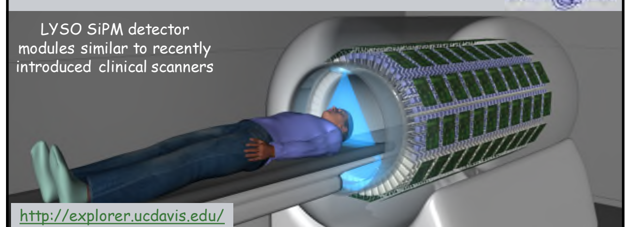

EXPLORER is a multi-institutional NIH funded consortium established to design, develop and construct the world's highest sensitivity whole body PET scanner.

- University of California at Davis
- Lawrence Berkeley National Laboratory
- University of Pennsylvania.

Jan 2017: United Imaging Healthcare (UIH) America and SensL Technologies of Cork, Ireland were selected to build the EXPLORER using silicon photomultiplier light sensors

Jan 2019: US Food & Drug Administration (FDA) clearance of the uEXPLORER total-body scanner.

V.B.4.c – EXPLORER project

United Imaging Healthcare expects production of U.S.-based systems to take place at its new facility in Houston by the end of 2019.

Detector Electronic Readout Modules

V.B.4.c – EXPLORER project

Present 'whole' body PET scanners (A) have poor sensitivity (<1%). Even for tissue inside the ring, only about 3-5% of the signal is collected. A 40-fold gain in sensitivity is realized with the 'total'-body PET scanner (B)

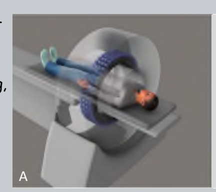

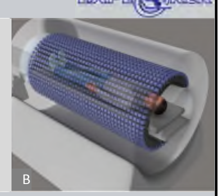

Additional increases in sensitivity are anticipated from improved timing resolution, Δt.

$$SNR \propto \frac{1}{\sqrt{\Delta t}}$$

400 ps : Recent commercial PET scanners

200 ps: Prototype clinical scanners

100 ps: Benchtop timing experiments

Cherry SR et. Al., Total-Body PET..., J. Nucl. Med., Jan 2018